Surface modification of silicate, borosilicate and phosphate bioactive glasses to improve/control protein adsorption: PART I

Ceramics International 49 (2023) 1261–1275

Contents lists available at ScienceDirect

Ceramics International

journal homepage: www.elsevier.com/locate/ceramint

Surface modification of silicate, borosilicate and phosphate bioactive glasses to improve/control protein adsorption: PART I

Virginia Alessandra Gobbo [a,*], Vijay Singh Parihar [a], Mirko Prato [b], Minna Kellomäki [a], Enrica Vernè [c], Silvia Spriano [c], Jonathan Massera [a]

[a] Faculty of Medicine and Health Technology, Tampere University, 33720, Tampere, Finland
[b] Nanochemistry Department, Istituto Italiano di Tecnologia, Via Morego 30, 16163, Genova, Italy
[c] Department of Applied Science and Technology, Politecnico di Torino, 10129, Torino, Italy

ARTICLE INFO

Keywords:
Bioactive glasses
Surface modification
Surface charge
Surface reaction
Surface physico-chemical properties

ABSTRACT

Bioactive glasses (BGs) are promising for bone tissue regeneration. BG composition can be tailored, according to the application of interest, and/or functionalized with organic molecules/biomolecules to improve their performances. However, despite the wide knowledge concerning BGs, their interaction with proteins, fundamental for controlling the fate of the implant, has not been deeply investigated yet. Controlling or predicting protein adsorption requires a full understanding of the materials surface physico-chemical properties. In this work, four different BGs (S53P4, B25, SCNB, PhGlass) were surface-modified by four different treatments: 72 h-soaking in TRIS, 72 h soaking in simulated body fluid, APTES grafting and quaternized APTES grafting. The surfaces were then characterized both untreated and after each treatment by contact angle, zeta potential analysis, X-ray photoelectron spectroscopy, Fourier Transform InfraRed–Attenuated Total Reflectance spectroscopy and Scanning Electron Microscopy and Energy Dispersive Spectroscopy. Inductively Coupled Plasma – Optical Emission Spectrometry was then performed to investigate the ion leaching. The aim of this study (Part I) is the physico-chemical characterization of BGs as a function of the implemented treatments, aiming to better understand how the superficial properties are successively affecting protein adsorption. Protein adsorption on untreated and treated BGs will be discussed in a following manuscript (Part II).

1. Introduction

Bioactive glasses (BGs), pertaining to their high versatility allowing to tailor their composition and, consequently, their properties, are a promising class of biomaterials for applications ranging from bone regeneration to soft tissue engineering [1–3]. The first BG (45S5 Bioglass®) was designed between 1969 and 1970 by Larry L. Hench [4]. 45S5 is a silicate glass able to induce the formation of a polycrystalline layer of hydroxyapatite – the main inorganic component of hard tissues – on its surface when in contact with body fluids [4]. Since the discovery of the first bioactive glass by L.L. Hench, many researchers have focused on modifying the glass composition to tailor the glass dissolution rate and mechanism or to enable the control release of therapeutic ions. As examples, specific ions, such as silver, copper and strontium, were reported to, respectively, promote antimicrobial activity, angiogenesis and bone remineralization [5–7]. The mechanism of dissolution/-reaction of silicate bioactive glasses has been heavily discussed in the past and can be summarize as follow. The release of Na^+ ions from the BG and the hydration of its surface leads to the formation of Si–OH groups, whose polycondensation conducts to the formation of Si–O–Si bonds; this layer, which is forming on the top surface of the material, at the interface with the surrounding environment, is referred to as silica-rich layer. Such hydrated silica-rich layer appears to be a good substrate for the adsorption of Ca^{2+} ions, phosphate, and carbonate groups. These chemical moieties crystallize and, around 5–6 h after the implantation of the material, hydroxyapatite/hydroxycarbonate apatite (HA/HCA) is formed on the BG surface. The formation of HA/HCA favors the interaction with the biomolecules which are present in the surrounding environment, mainly proteins. However, silicate BGs have two main drawbacks. First, their dissolution is incongruent, which means that the composition of the material is varying both overtime and over the depth of the material itself [8,9]. This leads to a limited control over the dissolution process and over the composition of the material during dissolution [10]. The second issue is related to the sensitivity of

* Corresponding author.
E-mail address: virginiaalessandra.gobbo@tuni.fi (V.A. Gobbo).

https://doi.org/10.1016/j.ceramint.2022.09.105
Received 7 July 2022; Received in revised form 8 September 2022; Accepted 8 September 2022
Available online 19 September 2022

silicate BGs to crystallization, particularly critical during sintering process, when temperatures close or even above the crystallization onset temperature are reached. Uncontrolled crystallization of a bioactive glass is known to lead to a decrease or even the suppression of the bioactivity [10–12]. Consequently, various BG compositions have been tailored and tested so far to solve these issues and add/optimize BG properties [13–15]. Borosilicate BGs have been widely studied as they enable sintering without significant crystallization and are also known to promote chondrogenesis, which could be of particular interest for future musculoskeletal applications [13,16]. Tailoring boron content in BG composition also affects the bioactivity of the material itself. The glass is degrading and inducing HA/HCA precipitation at a rate that is a function of the amount of boron: the higher the boron content in bioactive borosilicate glasses, the faster the dissolution rate, and the higher the thickness of the precipitated HA layer [17,18]. Furthermore, boron has been discovered to promote angiogenesis, which is fundamental for the vascularization of the just regenerated tissue and, consequently, for the health of the new tissue itself and the success of the implant [19,20].

In order to avoid the non-congruent dissolution phenomenon typical of silicate BGs, another class of BGs was introduced, i.e. phosphate glasses. Phosphate glasses (especially in the metaphosphate domain) are dissolving congruently. Maintaining the same composition overtime and over the depth of the material during the dissolution constitutes an advantage considering the higher control over the dissolution and ion release [14,15]. Moreover, boron in phosphate glasses was also found to limit the formation of crystals during sintering process, significantly increasing the crystallization onset temperature of the material [13,21].

While many different types of BGs have been developed for various applications, the BG surface chemistry and its impact on protein adsorption has not been extensively studied. Protein adsorption is a crucial step for the successive cell adhesion: the adsorption of specific biological moieties promotes the adhesion of specific cells, leading to the development of a certain tissue, and this can consequently conduct to either the success or the failure of the implant [22]. However, to control or even predict the protein/material interaction, one should thoroughly understand the surface physico-chemical properties of the studied materials.

BG surface can be tailored by implementing specific treatments or functionalizations. Surfaces can be activated by washing and/or sonicating them to expose functional groups. Furthermore, specific molecules can be grafted, or the precipitation of new phases can be induced. The final goals are multiple, ranging from the improvement of biocompatibility to the control over bioactivity, the addition of ulterior therapeutical properties according to the final applications, and the increase of the affinity to chemical moieties or biological systems of interest [23–27]. Recent studies [27–29] have demonstrated how pre-conditioning BGs, incubating them into buffer solutions for a specific time, induces a higher biocompatibility. Prevention of ion burst release and the precipitation of a calcium phosphate (CaP) layer are limiting the potentially toxic strength of the released ions flux when in contact with cells. Antimicrobial properties could be also imparted to the substrates by implementing specific treatments aiming at the incorporation of ions on the surface of interest. Doping BGs with therapeutical ions permits to obtain a high concentration gradient, leading to an efficient antibacterial activity [26,30,31]. Other studies have demonstrated how to improve the affinity between the BG substrate and molecules of interest by inducing preferential interactions with the treated surface. Grafting specific molecules as coupling agents, such as 3-aminopropyltrietoxysilane (APTES) [23,25] or glutaraldehyde [32], exposes amine groups at the BG surface, thus enhancing protein adsorption. As previously discussed, protein adsorption constitutes a fundamental step for determining the success of the implant. The presence of specific proteins on the surface of the implant promotes the adhesion of specific cell types and the formation of healthy tissue, while, indirectly, limiting also the risk of infections. The control over this phenomenon is crucial in enhancing the regeneration of the tissue of interest [22].

In the current study, four BG compositions (two silicate, one borosilicate and one phosphate glass) were processed and treated by either pre-incubation (in TRIS or SBF) or functionalization (using APTES or Q-APTES). This manuscript focuses on the impact of the surface treatment on the BG physico-chemical properties. It will then be followed by a thorough study on protein adsorption. The relationship between surface chemistry and protein adsorption will be discussed.

2. Materials and methods

2.1. Bioactive glasses (BG)

The nominal composition of the BGs (S53P4, B25, SCNB and PhGlass) of investigation is reported in Table 1.

All glasses were produced by the standard melt-quench method. The precursors used to produce the glasses were 1) Belgian quartz sand (SiO_2), ($CaHPO_4$).$2H_2O$, H_3BO_3, Na_2CO_3 and $CaCO_3$ for the silicate and borosilicate glasses and 2) Belgian quartz sand (SiO_2), $Ca(PO_3)_2$, NH_6PO_4, $(NaPO_3)_6$, $SrCO_3$ and MgO for the phosphate glass. The protocol to produce $Ca(PO_3)_2$ can be found in Ref. [33].

Appropriate amount of precursors were weighted and mixed in an alumina mortar. Melting of the silicate and borosilicate glasses was conducted in a platinum crucible while the phosphate glass was melted in a silica crucible. The melting temperatures and times are reported in Table 2. To melt S53P4, SCNB and PhGlass, the final melting temperature was directly set at the beginning of the process, while two intermediate temperatures were imposed for B25 and maintained for 30 min before reaching the final melting temperature. In all cases, the heating rate was set at 15 °C/min. Midway to the melting, the melts were mixed to ensure high homogeneity. At the end of the melting, the melts were cast inside a pre-heated (at 360 °C) graphite cylindrical mold. Rods with 10 and 14 mm diameter were prepared. The casted BGs were then annealed at temperatures that were established based on the glass composition as shown in Table 2 and let to cool down to room temperature.

The annealed rods were cut into discs with a thickness of 2 mm and then polished with SiC sandpapers (#320, #500, #800, #1200, #2500, #4000). The samples were stored in multi-well plates at room temperature (RT) inside a dry box before further testing.

2.2. BG pre-treatments

2.2.1. Soaking in TRIS and simulated body fluid (SBF) solutions

TRIS buffer solution (0.05 M) was prepared by dissolving 1.66 g of Trizma® Base (Trizma® Base, Primary standard and Buffer, ≥99.9% (titration), crystalline, Sigma Aldrich) and 5.72 g of Trizma® HCl (Trizma® hydrochloride, reagent grade, ≥99.9% (titration), crystalline, Sigma Aldrich) in 1 L of distilled water. The solution was let to stabilize for 3 h and the pH was 7.40 ± 0.02 at (37.0 ± 0.2) °C.

SBF was prepared according to Kokubo's protocol [34], dissolving each precursor in the proper order (1–8) in 1 L of distilled water, as reported in Table 3. The final pH was adjusted to 7.40 ± 0.01 at (36.5 ± 0.1) °C, by buffering the solution with Trizma® Base (6.118 g) and 1 M hydrochloric acid.

The treatment with TRIS and SBF solutions was implemented by

Table 1
BG nominal composition (%mol).

	SiO_2	P_2O_5	B_2O_3	Na_2O	CaO	SrO	MgO
S53P4	53.85	1.72		22.66	21.77		
B25	40.39	1.72	13.46	22.66	21.77		
SCNB	55.60			22.70	21.70		
PhGlass	2.50	45.00	2.50	10.00	20.00	10.00	10.00

Table 2
BG melting parameters.

	Melting temperature (°C)	Melting time (hours)	Annealing temperature (°C)	Annealing time (hours)
S53P4	1375	1	500	8
B25	(650 – 30 min) (850 – 30 min) 1250	1	500	8
SCNB	1450	2	550	10
PhGlass	1000	1	425	8

Table 3
Precursors for SBF preparation.

1	NaCl	8.035 g
2	$NaHCO_3$	0.335 g
3	KCl	0.225 g
4	K_2HPO_4. $3H_2O$	0.231 g
5	$MgCl_2$. $6H_2O$	0.311 g
6	1 M − HCl	39 ml
7	$CaCl_2$. $2H_2O$	0.308 g
8	Na_2SO_4	0.072 g

TRIS and SBF solutions were stored at 4 °C.

soaking each BG disc in 50 ml of solution, respectively, and incubated for 72 h at 37 °C. After that, the samples were removed, dried and stored in multi-well plates at RT inside a dry box before further analysis. For all the experiments, a control (solution without any samples) was kept under the same conditions. Both the controls and the sample solutions were characterized by measuring pH values (Mettler Toledo, Seven Multi) and by inductively coupled plasma – optical emission spectrometry (ICP-OES). ICP-OES (5110 ICP-OES, Agilent Technologies) was conducted for the purpose of evaluating the concentration of the elements inside the solutions of interest. As such, 1 ml of the immersion solution was pipetted and diluted in 9 ml ultra-pure 1 M HNO_3. Table 4 reports the evaluated elements and the relative wavelengths used for their quantification.

The measurement was implemented on 6 samples per condition.

2.2.2. Silanization

The aim of silanization was to increase the affinity between the BG surface and the protein by exposing amine groups on the substrates to optimize the adsorption process. 3-Aminopropyltriethoxysilane (APTES, 99%, Sigma-Aldrich) was grafted to the BG surface using the procedure described in Refs. [35,36]. Shortly, BGs (6 samples per batch) were sonicated 5 min in acetone (one time) and then in distilled water (three times) to be washed; after this, they were soaked in 150 ml ethanol (96% vol., VWR) with 70 μl APTES (2 mM) for 6 h at RT, dried for 1 h at 100 °C, sonicated in ethanol for 5 min and finally dried again for 1 h at 100 °C.

Aside from the traditional APTES grafting, samples were also functionalized with quaternized APTES (Q-APTES) [37], as reported in Figs. S1 and S2.

In order to synthesize Q-APTES, 5 ml of APTES (APTES, Sigma-Aldrich, 99%) was poured into a 100 ml sealed tube and 50 ml of dry chloroform (≥99.8%, Honeywell) was then added. To the stirred solution of APTES, 10 ml of 1-hexylbromide (98%, Sigma Aldrich) was added under inert atmosphere. The pressure tube was closed with reaction mixture and refluxed at 50 °C for 24 h. As the reaction proceeded, the precipitation of the product was observed as it is characterized by very low solubility in chloroform. The reaction was monitored by thin-layer chromatography (TLC). After the completion of the reaction, the reaction mixture was transferred to 100 ml round bottom flask and the solvent was removed from the rotary evaporator (55 °C, 185 rpm) which led to the obtention of a light brown highly viscous compound. The extracted crude product was then washed with chloroform followed by ethyl acetate (Ethyl acetate, Merck KGaA) to remove unreacted APTES. The samples were sonicated for 5 min in each solvent, respectively, and dried 3 times. The washed pure product was characterized by proton and carbon nuclear magnetic resonance (NMR) spectroscopy. All NMR spectra (^{1}H-NMR and ^{13}C-NMR) were acquired using a JEOL-500 MHz (SCZ500R, JEOL Resonance, Japan) using $CDCl_3$ and CD_3OD as solvents. The spectra are presented in the supporting information (SI).

Before grafting on BG surfaces, the extracted compound was finally maximum dried in the rotary evaporator under vacuum at 55 °C and 185 rpm, for 2 h. The coumpond was then placed in the vacuum oven at 37 °C, overnight. To functionalize the glasses, 70 mg of Q-APTES was weighted and dissolved, overnight, in 150 ml ethanol at 50 °C under stirring at 400 rpm. To graft Q-APTES on the BG surfaces the same protocol used for APTES was implemented.

All the silanized samples (both the APTES- and Q-APTES-pretreated) were stored in multi-well plates in a dry box before further analysis.

Table 4
Elements of interest for ICP-OES and relative wavelengths.

Element	Wavelength (nm)
Si	251.432
Ca	317.933
P	213.618
Na	588.995
B	249.678
Mg	285.213
Sr	421.552

2.3. Substrates characterization

2.3.1. Contact angle analysis

The contact angle analysis was performed aiming to evaluate the wettability of the substrates. The measures were implemented on 10 mm-diameter BG discs in static conditions by the sessile drop method using Theta Line tensiometer, Biolin Scientific. A 5 μl-drop of ultrapure water was gently deposited on the surface of the sample of interest through a syringe. A 10 s video with a rate of 20 frames/s was recorded and analyzed by OneAttension Software. The measurements were done in triplicate.

2.3.2. Zeta potential analysis

Zeta potential analysis was performed by an electrokinetic analyzer (SurPASS3, Anton Paar). A solution of 1 mM KCl was prepared as electrolyte dissolving KCl (Potassium chloride, 100%, VWR) in ultra-pure water. The untreated and pre-treated samples were analyzed as 14 mm-diameter discs using the Adjustable Gap Cell. Inside the cell, two samples were placed parallelly with an optimized gap of 100 μm. For each BG condition, the zeta potential value at physiological pH (7.4) was acquired to evaluate the eventual variations in the surface charge after the four implemented pre-treatments. The pH was set by automatically buffering the electrolyte solution with two buffer solutions, respectively 0.05 M HCl and 0.05 M NaOH solution. Each measurement consisted in three cycles of zeta potential analysis, around 90 s long each for a total of 4.5 min per condition. The experiment was conducted in triplicate.

2.3.3. X-ray photoelectron spectroscopy (XPS)

XPS analyses were performed with a Kratos Axis Ultra^{DLD} spectrometer, to evaluate the effectiveness of silanization of BGs. Silanized samples, respectively with APTES and Q-APTES, have been analyzed and untreated samples have been tested as control. All the analyses were conducted using a monochromatic Al Kα source ($h\nu$ = 1486.7 eV), operated at 20 mA and 15 kV. Survey spectra were acquired at pass energy of 160 eV, over an area of (300 x 700) μm^2. High-resolution spectra of silicon (Si 2p), oxygen (O 1s), carbon (C 1s), nitrogen (N 1s) and bromine (Br 3d) regions were then acquired to evaluate the presence

of grafted APTES and Q-APTES on the surfaces of interest. In the Results and discussion, the focus was on nitrogen, oxygen and bromine. For to compensate the charging effect, the Kratos charge neutralizer system was used. The spectra were referenced setting the peak of hydrocarbon C 1s to 284.80 eV. The experiment was made in triplicate and three different areas were analyzed on each sample. Spectra were analyzed using CasaXPS software (version 2.3.24) [38].

2.3.4. Fourier Transform InfraRed – Attenuated Total Reflectance (FTIR-ATR) spectroscopy

FTIR spectroscopy was performed using PerkinElmer Spectrum One FTIR Spectrophotometer (PerkinElmer, Waltham, MA) in ATR mode. The spectra were acquired within the wavenumber range 4000-650 cm^{-1}, setting the resolution at 1 cm^{-1}. Each spectrum was obtained by averaging 32 scans. All spectra were background-corrected and normalized to the band with highest intensity.

2.3.5. Scanning Electron Microscopy and Energy Dispersive Spectroscopy (SEM/EDS)

SEM/EDS (Leo 1530 Gemini, Zeiss and EDXA UltraDry, Thermo Scientific) analysis was performed on the surface and cross-section of the untreated and treated samples. EDS analysis was implemented for evaluating compositional change resulting from the surface treatments.

To evaluate the compositional change across the cross section (especially for sample treated in TRIS and SBF), samples were embedded in resin and the cross section of the samples was then polished.

Compositions are reported in %mol (with an accuracy of ±1.5 % mol).

3. Results and discussion

The wettability of BGs was evaluated through contact angle (CA) analysis on the four compositions (S53P4, B25, SCNB, PhGlass) combined with the five surface treatments (bare, TRIS, SBF, APTES, Q-APTES). The results are reported in Fig. 1.

Overall, it is possible to notice a significant variation of CA values on the treated surfaces, compared to the bare ones, which means that all the surface-modifications have been implemented successfully. All the BG compositions present an analogue response to TRIS/SBF soaking and to silanization (APTES/Q-APTES), respectively. After soaking in TRIS/SBF, CA values are significantly decreasing, compared to the bare samples, suggesting an increase in hydrophilicity of the substrates after these treatments. This can be explained by the strong hydration characterizing TRIS-treated samples and the possible precipitation of HA/HCA [25]. For all the compositions, there is no statistical difference between TRIS- and SBF-treated BGs, except for S53P4, whose wettability is higher after soaking in SBF than after soaking in TRIS. After silanization, on the contrary, the substrates present a significant increase in CA values, suggesting a strong decrease of hydrophilicity on both APTES- and Q-APTES-treated surfaces. This can be due to the presence of both hydrophobic organic chains (carbon backbone) of silanes and exposed amines, both protonated and not, on the analyzed surfaces [35]. On PhGlass the values are statistically comparable between APTES- and Q-APTES-treated samples, while on silicate and borosilicate BGs it is possible to notice a significant difference between them, especially for B25 and SCNB, on which Q-APTES grafting induces a stronger decrease in surface wettability. However, it is important to highlight that all the analyzed samples are still hydrophilic, since all the values are lower than 90°.

The surface zeta potential of the considered BGs was then evaluated considering the four compositions (S53P4, B25, SCNB, PhGlass) combined with the five surface treatments (bare, TRIS, SBF, APTES, Q-APTES), as reported in Fig. 2. The values were recorded at pH = 7.4.

First of all, the zeta potential of the bare silicate (S53P4, SCNB) and borosilicate (B25) BGs ranged from −47.88 to −23.86 mV, in agreement with previously reported values [25,39]. PhGlass showed a more intense negative charge on its surface, reaching −60.65 mV.

According to the obtained results, the four surface treatments on the considered BG compositions were implemented successfully, since a statistically significant variation of zeta potential values is evident. All the treatments induced a reduction of the absolute value of the zeta potential of the analyzed surfaces. Concerning TRIS and SBF, one can justify the decrease in zeta potential with the formation of the silica-rich layer and the possible precipitation of a reactive layer, able to shield the negative charges exposed by the surface of the BGs [25]. The reduction of the absolute value of the zeta potential is always larger on the SBF-treated samples than on the TRIS-treated ones, phenomenon explainable by the thicker HA/HCA layer precipitating at the surface of this materials in such condition [40]. This is further supported by the fact that B25, the most reactive BG composition, exhibits the lowest absolute value of zeta potential, very close to a null net charge. Indeed, this bioactive glass is expected to lead to a thicker reactive layer than S53P4 and SCNB upon immersion in SBF or TRIS [25]. As reported in previous works, the presence of a thick HA/HCA layer, especially after immersion in SBF, is inducing a very low absolute value of zeta potential

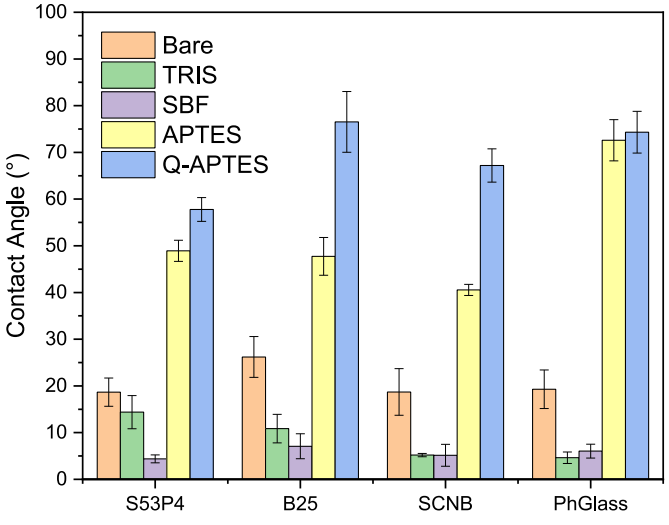

Fig. 1. CA analysis at the surface of the glasses S53P4, B25, SCNB and PhGlass, untreated and surface-treated with TRIS, SBF, APTES and Q-APTES.

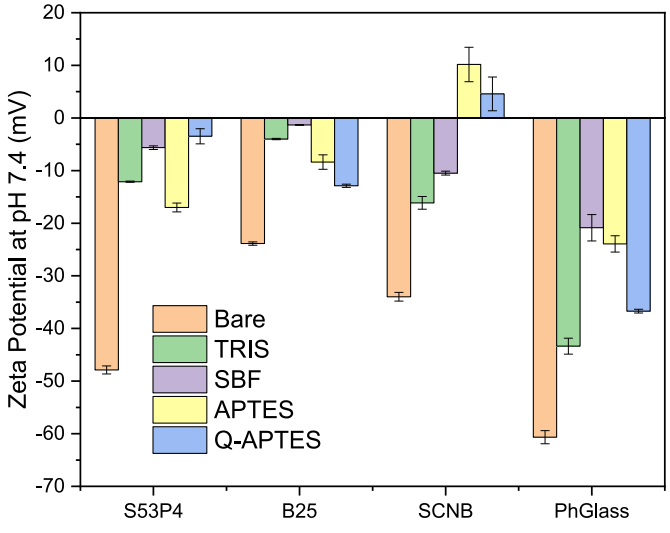

Fig. 2. Zeta potential analysis on the surface of S53P4, B25, SCNB and PhGlass, untreated and surface-treated with TRIS, SBF, APTES and Q-APTES, at the physiological pH (7.4).

[40].

Concerning the silanized samples, a significant tendency towards an overall null net charge was observed on S53P4 and B25. It can be justified by the exposition of the positively charged amine groups by the grafted molecules (APTES/Q-APTES), which partially balances the negative charge of the substrates [25]. The silanized SCNB even shows an overall positive net charge, slightly more intense for APTES-treated samples (10.17 mV with respect to 4.58 mV for Q-APTES). The positive zeta potential of SCNB can be explained by the intrinsic lower reactivity of this composition. The higher stability leads to a more stable functionalization of the surface. The silanized PhGlass also showed a lower absolute value of the zeta potential compared to the bare substrate. This could be due to grafting of APTES and Q-APTES not only through the methyl groups, but also through the amine groups, because of the higher absolute value of the zeta potential of the substrate, exposing then a lower amount of the positively charged groups [41–43].

A correlation between zeta potential and CA values was observed on the considered BGs after soaking in TRIS and SBF. Generally, the decrease in CA characterizing TRIS- and SBF-treated samples, compared to the untreated surfaces, was associated to an increase in zeta potential. This could be explained by the hydration of the top layer and the precipitation of HA/HCA [25]. On the other hand, no strong correlation between zeta potential and CA was observed on the silanized samples, neither with APTES nor Q-APTES. This is most likely linked to APTES/Q-APTES grafting density and to the exposition of both negative and positive charged functional groups on these surfaces.

The effectiveness of BG silanization with APTES and Q-APTES molecules respectively grafted on the surfaces of interest were investigated by XPS. High-resolution spectra were acquired to evaluate the presence of nitrogen (N 1s, Fig. 3) and oxygen (O 1s, Fig. 4) on APTES- and Q-APTES-treated BGs. Bromine (Br 3d) high-resolution spectra are also reported in Fig. 5 to confirm Q-APTES integrity upon grafting on all the considered substrates (S53P4, B25, SCNB, PhGlass).

XPS analysis shows an overall homogeneous composition intra- and inter-sample. Silicon (Si 2p) signal is present on all bare silicate and borosilicate BGs (S53P4, B25, SCNB) surfaces. After silanization, both with APTES and Q-APTES, the intensity of the Si 2p peak increases, as expected due to the presence of silane groups in APTES and Q-APTES. On the bare PhGlass, instead, Si 2p peak is not detectable on the survey scan (not reported), probably because of its low content. However, a strong Si 2p signal was recorded after silanization (APTES/Q-APTES), with an intensity comparable to the silanized silicate and borosilicate BGs. Furthermore, in the case of B25 and SCNB, after silanization (APTES/Q-APTES) it is possible to observe an overall decrease of the content of calcium and sodium, and, in the case of PhGlass, also of magnesium and phosphorus. This can be attributed to the partial release

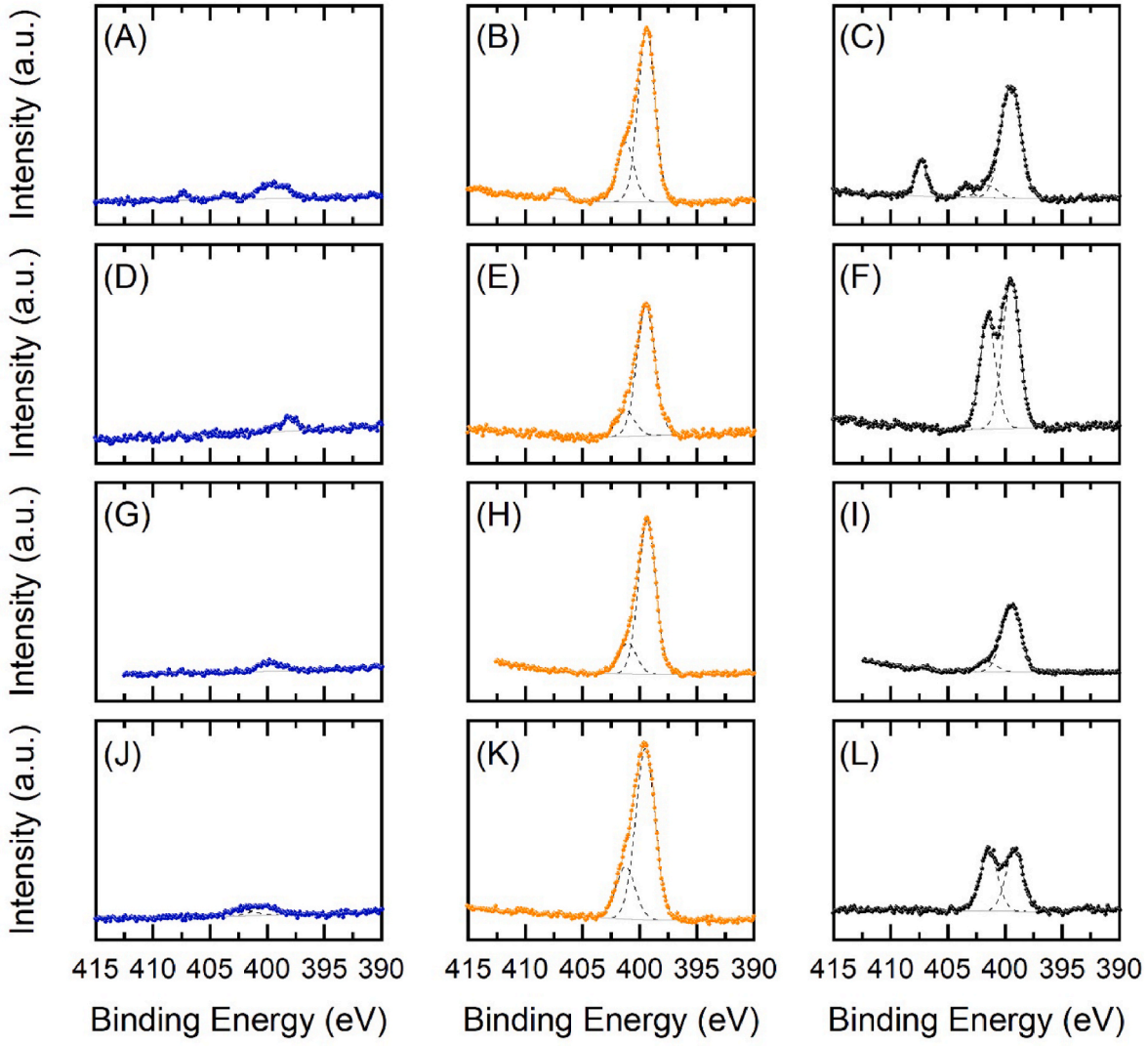

Fig. 3. XPS high-resolution spectra of N 1s acquired on: (A) bare, (B) APTES-treated and (C) Q-APTES-treated S53P4; (D) bare, (E) APTES-treated and (F) Q-APTES-treated B25; (G) bare, (H) APTES-treated and (I) Q-APTES-treated SCNB; (J) bare, (K) APTES-treated and (L) Q-APTES-treated PhGlass.

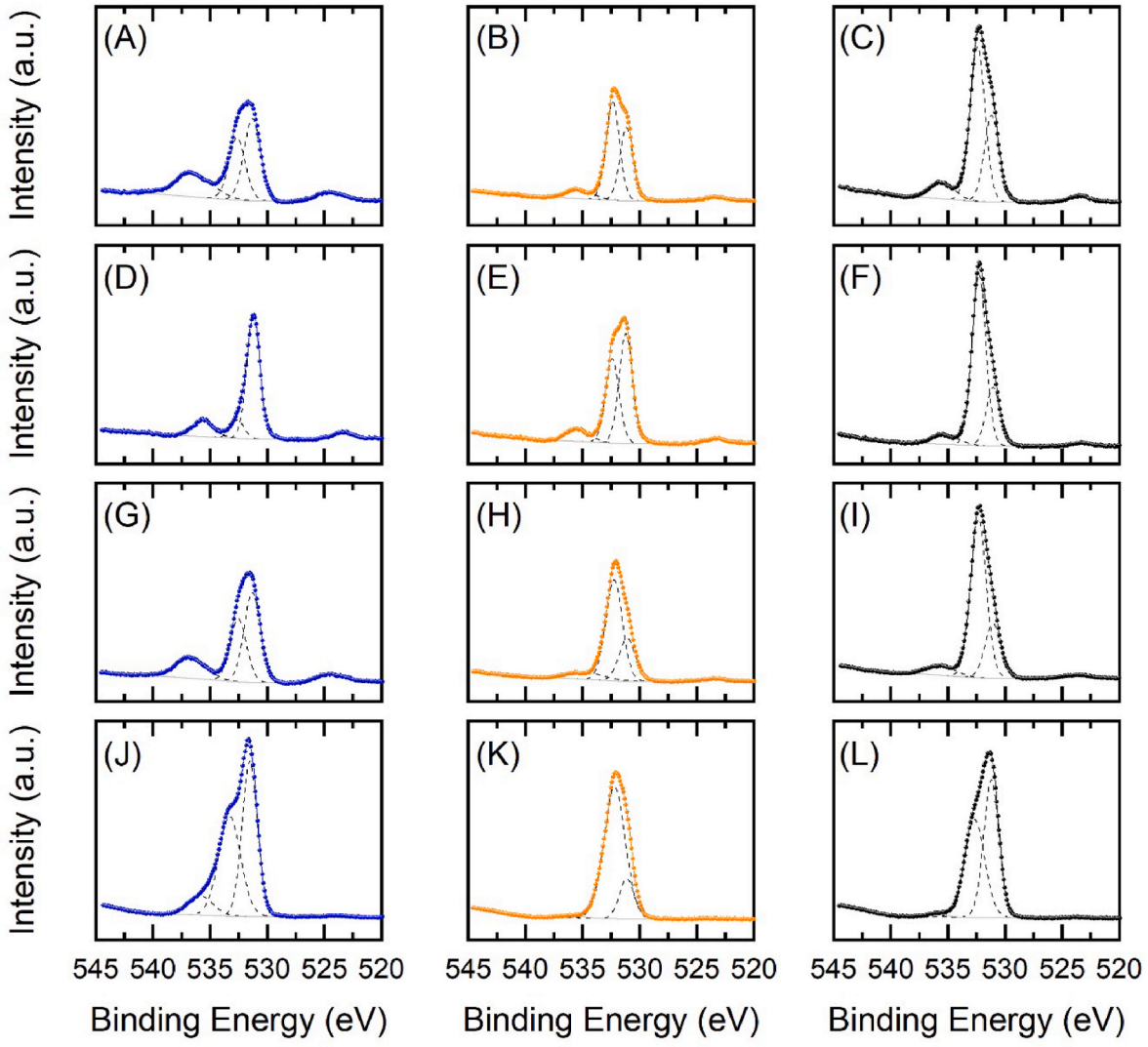

Fig. 4. XPS high-resolution spectra of O 1s acquired on: (A) bare, (B) APTES-treated and (C) Q-APTES-treated S53P4; (D) bare, (E) APTES-treated and (F) Q-APTES-treated B25; (G) bare, (H) APTES-treated and (I) Q-APTES-treated SCNB; (J) bare, (K) APTES-treated and (L) Q-APTES-treated PhGlass.

of these ions during the silanization process.

From Fig. 3 and from the survey scan (not shown here), nitrogen content [N] is very low and not homogeneous on S53P4, B25 and SCNB bare surfaces, 0.36 atomic % on S53P4, and even not detectable on B25 and SCNB. The presence of nitrogen is due to impurities [25]. A weak N 1s signal is present on bare PhGlass spectrum, with an intensity comparable to the Si 2p one. As said for the silicate and borosilicate, [N] significantly increases post functionalization with APTES and Q-APTES.

In more details, N 1s is present on the bare S53P4 surface (Fig. 3(A)) in three oxidation states: the main peak (~399.4 eV) can be attributed to organic N (e.g. amines) [25], while the other peaks at around 403.7 and 407.3 eV are consistent respectively with nitrites and nitrates [44]. In the case of bare B25 (Fig. 3(D)), the only contribution (~398.2 eV) might be related to aromatic imines (R = N-R) [45]. However, due to the particularly low intensity of these peaks, it is reasonable to consider the presence of N on bare BGs as a surface impurity [25]. After silanization (APTES/Q-APTES), N 1s signal significantly increases. Silanized S53P4 (Fig. 3(B), (C)) presents three main contributions. The main peak at ~399.4 eV might be assigned to neutral amines (-NH_2), while a lower intensity peak (~401.0 eV) is attributed to protonated amines (-NH_3^+) [23,25]. The third component at 407.3 eV, assigned to nitrates, is present on both samples, but with higher intensity on the Q-APTES one, where a minor component at ~403.4 eV, assigned to nitrites, is also present. Silanized B25, SCNB and PhGlass exhibit only the first two peaks, attributed to neutral (~399.4 eV) and protonated (~401.0 eV) amines [23,25]. APTES-functionalized bioactive glasses are largely dominated by neutral amine groups. However, while this holds true also for APTES-grafted S53P4 and SCNB, the N 1s spectra of B25 and PhGlass clearly show a significant increase in protonated amines.

Fig. 4 presents the high-resolution spectra for oxygen, for all samples of investigation. It is possible to distinguish two main peaks on all the analyzed surfaces. In Table 5, the position of the O 1s peaks are reported with their relative amount, expressed in percentage (%) of the total peak area. The first component (referred to as Oxygen 1) is attributed to the hydroxyl groups (-OH) exposed at the surface of the material, while the second component (Oxygen 2) is assigned to Si–O bonds (~532.5 eV) in silicate and borosilicate glasses [23] while it is attributed to P–O–P bonds (~533.3 eV) in the case of the phosphate glass [35,46]. It is interesting to point out that the higher the OH content, the less electronegative the surface.

As appreciable in Fig. 4, the overall intensity of O 1s peaks are not significantly varying within the implemented conditions (bare and silanized BGs). However, a significant difference between the relative amount of the various Si species, as a function of the surface chemistry of the BG composition, is observable. Silicate and borosilicate BGs (S53P4, B25, SCNB) show a significant increase of Oxygen 2 species after

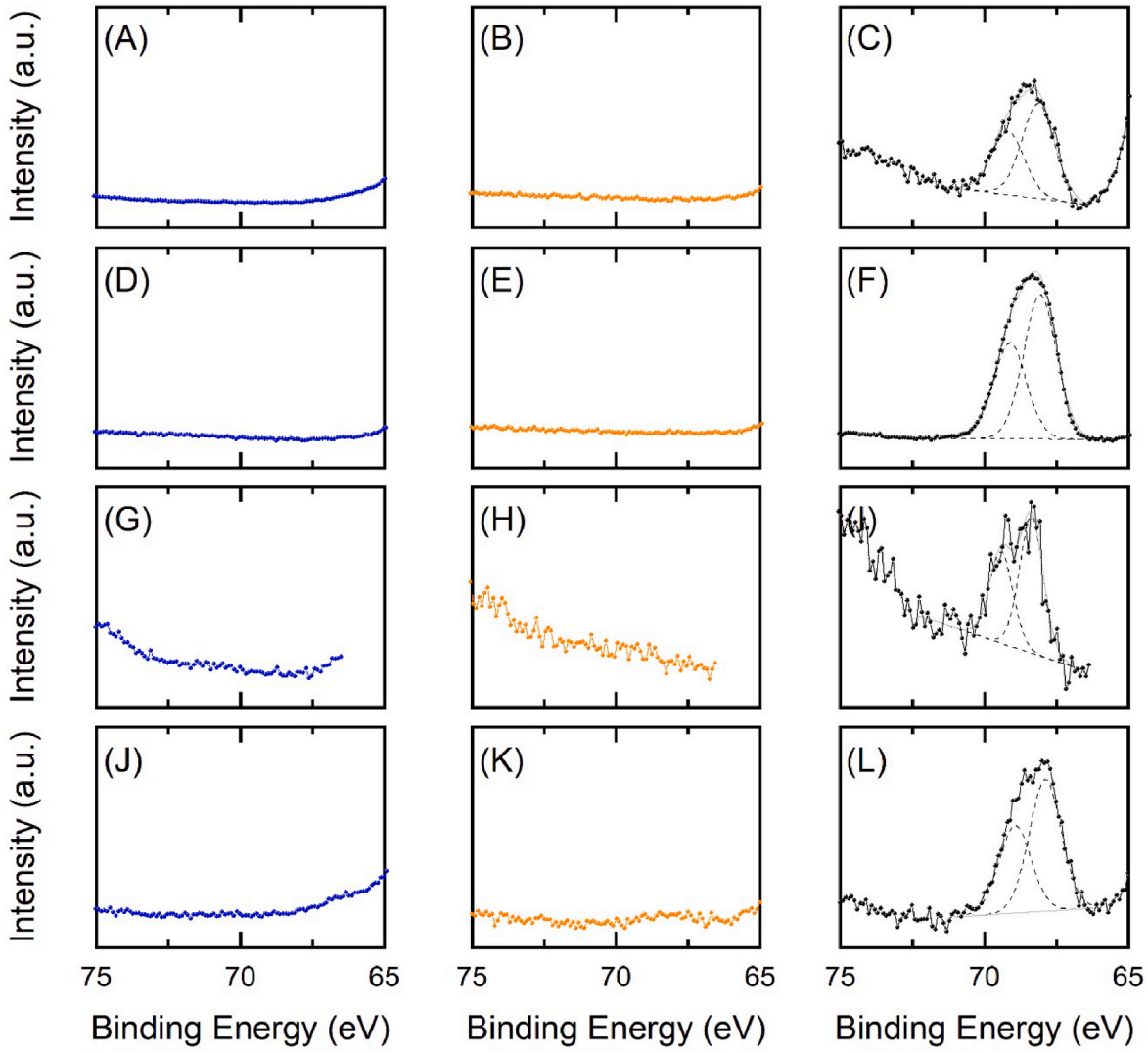

Fig. 5. XPS high-resolution spectra of Br 3d acquired on: (A) bare, (B) APTES-treated and (C) Q-APTES-treated S53P4; (D) bare, (E) APTES-treated and (F) Q-APTES-treated B25; (G) bare, (H) APTES-treated and (I) Q-APTES-treated SCNB; (J) bare, (K) APTES-treated and (L) Q-APTES-treated PhGlass.

silanization (APTES/Q-APTES). On the other side, the ratio between the two oxygen species for the untreated PhGlass is in agreement with previously published data [35]. Silanized PhGlass shows a significant difference between APTES- and Q-APTES-grafted samples. APTES-treated PhGlass presents a more intense Oxygen 2 component, while Oxygen 1 is predominant in the case of Q-APTES. Overall, it is possible to affirm that, according to the presented results, the silanization (APTES/Q-APTES), with a different density of grafted molecules in function of the BG composition, was successfully implemented on all the considered substrates.

Finally, high-resolution Br 3d spectra (Fig. 5) were evaluated to confirm the presence of bromine on the BGs surfaces after silanization with Q-APTES. The spectra acquired on all the considered BG compositions (S53P4, B25, SCNB, PhGlass) showed the characteristic Br 3d peak at ~71 eV, confirming the preservation of the element of interest also in the structure of the grafted molecule [47]. The intensity of Br 3d signal is not particularly intense on almost all the Q-APTES-treated surfaces (in average, one order of magnitude lower than Si 2p and N 1s peaks), with a characteristic amount ranging from 3 to 7% of N 1s. The only exception consists in B25, presenting a quantity of this element around the 39% of N 1s, and a ratio between Br 3d and protonated amines around 1:1. This is possibly due to the B25 showing the lowest electronegativity, compared to the other bare substrates, as seen in Fig. 2.

FTIR-ATR spectroscopy was implemented to evaluate the changes in the surface chemical structure of the studied BGs. The acquired spectra are presented in Fig. 6, where the comparison between the five treatments implemented on each BG composition is shown.

The bare silicate glasses (S53P4, B25, SCNB) exhibit three main peaks, a shoulder at 990 cm^{-1}, and two peaks at 867 and 740 cm^{-1}, respectively corresponding to Si–O–Si asymmetric stretching in SiO_4 units, carbonate groups vibration and Si–O bending [48,49]. B25 presents three additional peaks which confirm the presence of boron (B) in its structure: a peak at 1398 cm^{-1} attributed to BO_3 triangles, a shoulder at 1192 cm^{-1} due to BO_2O^- and a peak at 710 cm^{-1}, due to B–O–B stretching [25].

After soaking S53P4 and B25 in TRIS and SBF, the peaks characteristic of the bare silicate and borosilicate glasses (990, 867 and 740 cm^{-1}) are shifted towards higher wavenumbers (respectively to 1188, 1012 and 869 cm^{-1}). In the case of SCNB, this happens only after soaking in SBF. Other peaks are also visible. TRIS- and SBF-treated S53P4 and B25 present a broad band (3660 and 2220 cm^{-1}) assigned to O–H stretching vibration [50,51]. In the case of SCNB, such band was again only visible when the samples were soaked in SBF. Other peaks at 1420 and 1010 cm^{-1}, respectively corresponding to the carbonate and the phosphate groups [51,52], are detectable on SBF-treated silicate/borosilicate BGs.

Table 5
Oxygen components and their relative amount (%) on bare and silanized (APTES/Q-APTES) BGs (S53P4, B25, SCNB, PhGlass).

		S53P4		B25		SCNB		PhGlass	
		Position (±0.2 eV)	Relative amount	Position (±0.2 eV)	Relative amount	Position (±0.2 eV)	Relative amount	Position (±0.2 eV)	Relative amount
Bare	Oxygen 1	531.3 eV	56.90%	531.2 eV	86.8%	531.3 eV	58.8%	531.5 eV	52.0%
	Oxygen 2	532.6 eV	43.10%	532.6 eV	13.2%	532.5 eV	41.2%	533.3 eV	48.0%
APTES	Oxygen 1	531.1 eV	42.60%	531.2 eV	56.7%	531.1 eV	29.8%	531.0 eV	9.7%
	Oxygen 2	532.3 eV	57.40%	532.4 eV	43.3%	532.2 eV	70.2%	532.1 eV	90.3%
Q-APTES	Oxygen 1	531.2 eV	35.90%	531.1 eV	25.6%	531.1 eV	25.7%	531.2 eV	51.7%
	Oxygen 2	532.4 eV	64.10%	532.3 eV	74.4%	532.3 eV	74.3%	532.7 eV	48.3%

The change in surface chemical structure indicates that treatment in TRIS and SBF leads to the hydration of the silicate and borosilicate structure, followed by the precipitation of a reactive layer [53–55]. The absence of this reactive layer on TRIS-treated SCNB can be explained by the absence of phosphorus in SCNB composition [56].

Post silanization (with APTES or Q-APTES) the typical vibrations of the silicate and borosilicate structure are still visible. On S53P4 and SCNB surfaces additional peaks (at 1662 and 1621 cm^{-1}) are detectable confirming the efficient grafting of APTES and Q-APTES molecules. Indeed, these peaks have been attributed to NH_2 and NH groups, respectively [57,58]. Additional peaks at 1373 and 1354 cm^{-1}, are also present and can be assigned to C–O bond stretching [49]. Furthermore, a low intensity peak is visible on silanized S53P4 at 2779 cm^{-1} (not shown here), which is attributable to the carbon backbone of APTES and Q-APTES molecule [57]. It suggests that a more efficient silanization had place on the silicate BGs (S53P4, SCNB) than on borosilicate (B25), which is in accordance with previous studies [25].

In the case of the PhGlass (Fig. 6(D)), it is still possible to detect the three peaks characteristic of the silicate network (990, 867 and 740 cm^{-1}) despite the low content in SiO_2 in this glass composition, and carbonate groups [25,48,49]. However, other significant peaks are detectable at 1236 cm^{-1} corresponding to P–O–P stretching (non-binding oxygen, NBO, Q2) [59], at 1076 cm^{-1} corresponding to phosphate group [60], at 745 cm^{-1} attributable to P–O–P stretching (binding oxygen, BO, Q1) and at 600 cm^{-1} to P–O stretching (Q0) [59]. These peaks are characteristic of phosphate glasses [59]. Peaks related to borate network were not detected by the instrument, either due to the low content in B_2O_3 or the overlap of P–O–P and P–O–B vibrations [25,59]. Soaking in TRIS and SBF induced the formation of a hydrated layer confirmed by the presence of peaks at 3185 and 2990 cm^{-1}, attributable to O–H stretching vibrations [50,51]. Other peaks at 1630 and 1556 cm^{-1}, attributable to the combined effect of H–O–H and O═P–OH vibrations are also visible [61]. This suggests the formation of a reactive layer, most likely within the dicalcium phosphate dihydrate composition, on the surface of PhGlass [61]. Silanization did not affect the spectrum of the PhGlass, and since additional peaks are not detectable, this suggests a less efficient grafting of both APTES and Q-APTES molecules.

TRIS and SBF solutions, post-treatment, were analyzed by ICP-OES aiming to evaluate possible ion leaching/consumption occurring during the surface treatments. The balance between the ions released from each BG, the ones adsorbed on the surface of the sample and the ones precipitated at the interface, was estimated. In Fig. 7 the concentration of each element (Si, Na, Ca, P, B, Sr, Mg) in the uptake solutions is reported, expressed as part per million (ppm), and compared to the control solutions.

Silicon (Fig. 7(A)) was released in TRIS and SBF in a quite high amount by S53P4 without any statistical difference, with a concentration around 30 ppm in both solutions. B25 released more silicon in TRIS solution (30 ppm) than in SBF (23 ppm). SCNB, because of its higher stability, released in the solutions a lower amount of silicon, around 11 ppm, with no statistical difference between the two uptake solutions. Boron (Fig. 7(B)) was released by B25, in a slightly higher amount in TRIS than in SBF, with a final concentration in the uptake solutions of 18 and 11 ppm, respectively. Silicon and boron were released by PhGlass in a very low amount (close to zero), because of the initial low amount of silica (2.50 mol%) and boric oxide (2.50 mol%) in its composition.

Sodium release (Fig. 7(C)) was only quantified in TRIS solution since SBF already contains a substantial amount of sodium. Sodium release in TRIS was comparable between S53P4 and SCNB, with a concentration around 30 ppm. B25 released a higher amount of sodium (almost two times), while the amount released by PhGlass was close to zero.

The calcium release (Fig. 7(D)) in TRIS is characterized by an analogous trend, compared to the one of sodium release. S53P4 and SCNB released a lower amount of calcium (13 and 8 ppm, respectively), while B25 released a higher amount of this element (34 ppm). It is known, from past studies, that boron is immiscible with the silicate phase in

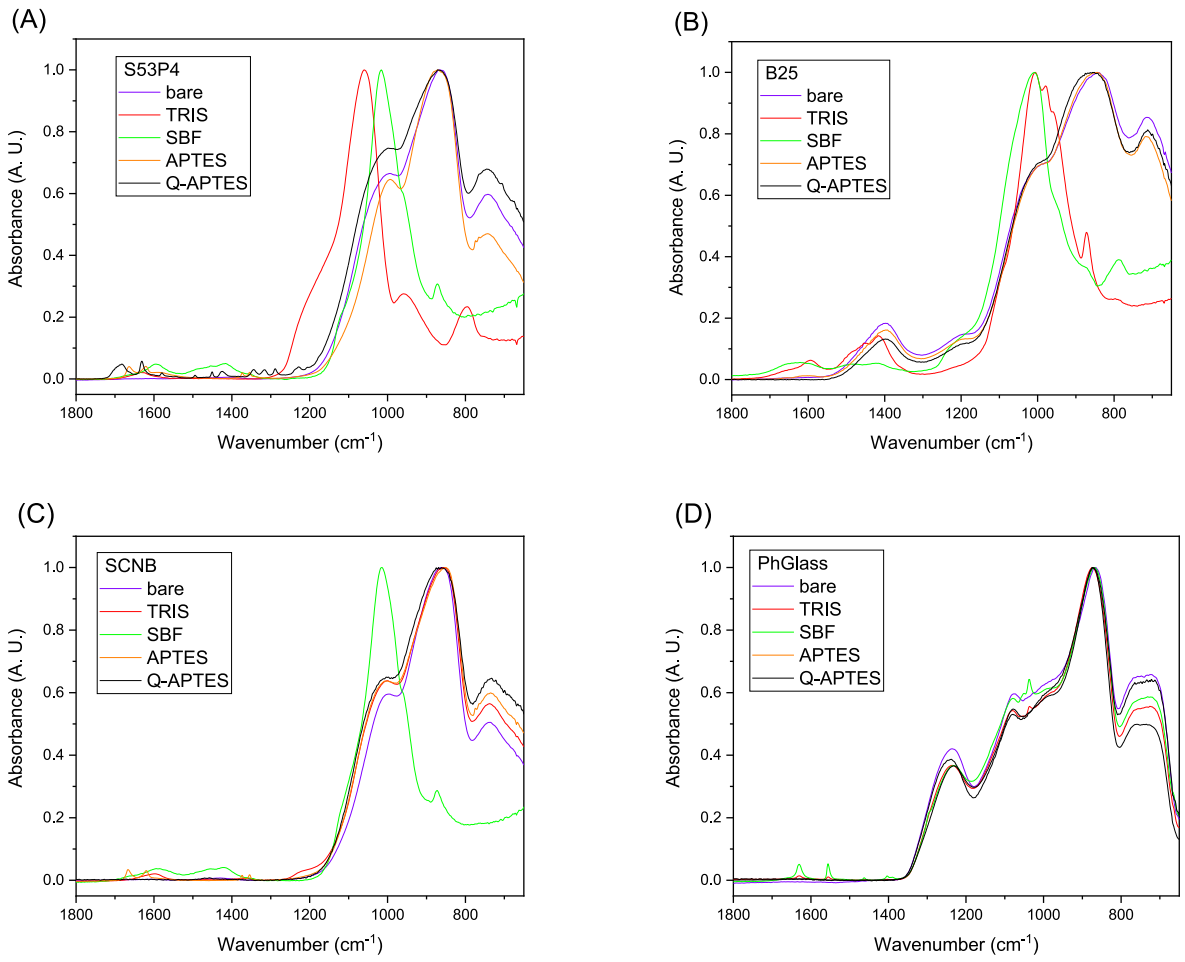

Fig. 6. FTIR-ATR spectra of (A) S53P4, (B) B25, (C) SCNB and (D) PhGlass, untreated and surface-modified (bare, TRIS, SBF, APTES, Q-APTES).

most compositions that are bioactive, leading to a phase separation (one phase rich in SiO_2 and one rich in B_2O_3) [62,63]. In addition, it was demonstrated that calcium ions have a preferential affinity to the borate phase [64]. Therefore, the faster dissolution of the borate phase, when compared to the silicate phase, can explain the higher calcium release in solution [62,63]. The quantity of released sodium and calcium in TRIS solution by PhGlass was instead close to zero and not detectable by the instrument. This can be justified by the different degradation process through which silicate/borosilicate and phosphate glasses are dissolving, respectively in an incongruent and congruent way [8,9,14,15]. Basically, because of the incongruent dissolution, when a silicate/borosilicate BG is soaked in a buffer solution (pH 7.4), sodium and calcium are released as first, while the other elements are released successively. This leads to a variation of the composition at the glass/liquid interface thus affecting the release dynamics during the soaking in TRIS and SBF [8]. [9]. On the contrary, since phosphate glasses are characterized by a congruent dissolution, they are degrading layer by layer, maintaining almost constant their composition overtime [65].

Instead, concerning calcium release in SBF, it is possible to notice a net increase of the content of this element in the SBF uptake solutions of S53P4, B25 and SCNB (around 80–90 ppm), compared to the SBF control solution (63 ppm), without any statistical difference between these three BG compositions. The opposite phenomenon is instead visible for the SBF uptake solution in which PhGlass was soaked, characterized by a net decrease of calcium concentration (until 23 ppm). This could mean that, during the surface reactions leading to silica-rich layer formation and HCA precipitation, silicate and borosilicate BGs are releasing a higher amount of calcium than the one which they adsorb in their network. On the other side, PhGlass, because of the significant concentration gradient with SBF, tends to adsorb a higher amount of calcium than the one that is released. This is in accordance with the hypothesis suggested by FTIR-ATR results (Fig. 6) about the precipitation of dicalcium phosphate diihydrate [61].

Magnesium (Fig. 7(E)) and strontium (Fig. 7(F)) are present only in the composition of PhGlass. While strontium was released in a low amount, leading to a final concentration close to zero in both the uptake solutions (TRIS and SBF), it is possible to observe a net decrease of magnesium concentration in the SBF uptake solution of PhGlass compared to the control one.

The concentration of phosphorus (Fig. 7(G)) in both TRIS and SBF does not present any significant difference between the control and the uptake solutions of silicate and borosilicate BGs, respectively (around 30 ppm). PhGlass had instead a different behavior. In TRIS, phosphorus, initially not detectable in the control solution, were mildly released to reach a final concentration of 4 ppm. A significant decrease in phosphorus concentration in SBF uptake solution (from 30 to 15 ppm) was detected. This suggests a net adsorption of this element and constitutes an ulterior confirmation about the formation of the dicalcium phosphate diihydrate layer on its surface [61].

BG surfaces were analyzed by SEM/EDS for the purpose to study the eventual variation of superficial morphology and topography after TRIS and SBF pre-treatment. The acquired images are reported in Fig. 8.

Comparing the bare samples and the soaked ones in TRIS/SBF, it is possible to appreciate a significant difference in the morphology for all the considered BG compositions (S53P4, B25, SCNB, PhGlass). The bare silicate and borosilicate substrates present a smooth surface. Both TRIS- and SBF-treated S53P4 and SBF-treated SCNB show a superficial layer of nanometric homogeneously-distributed grains, attributable to the

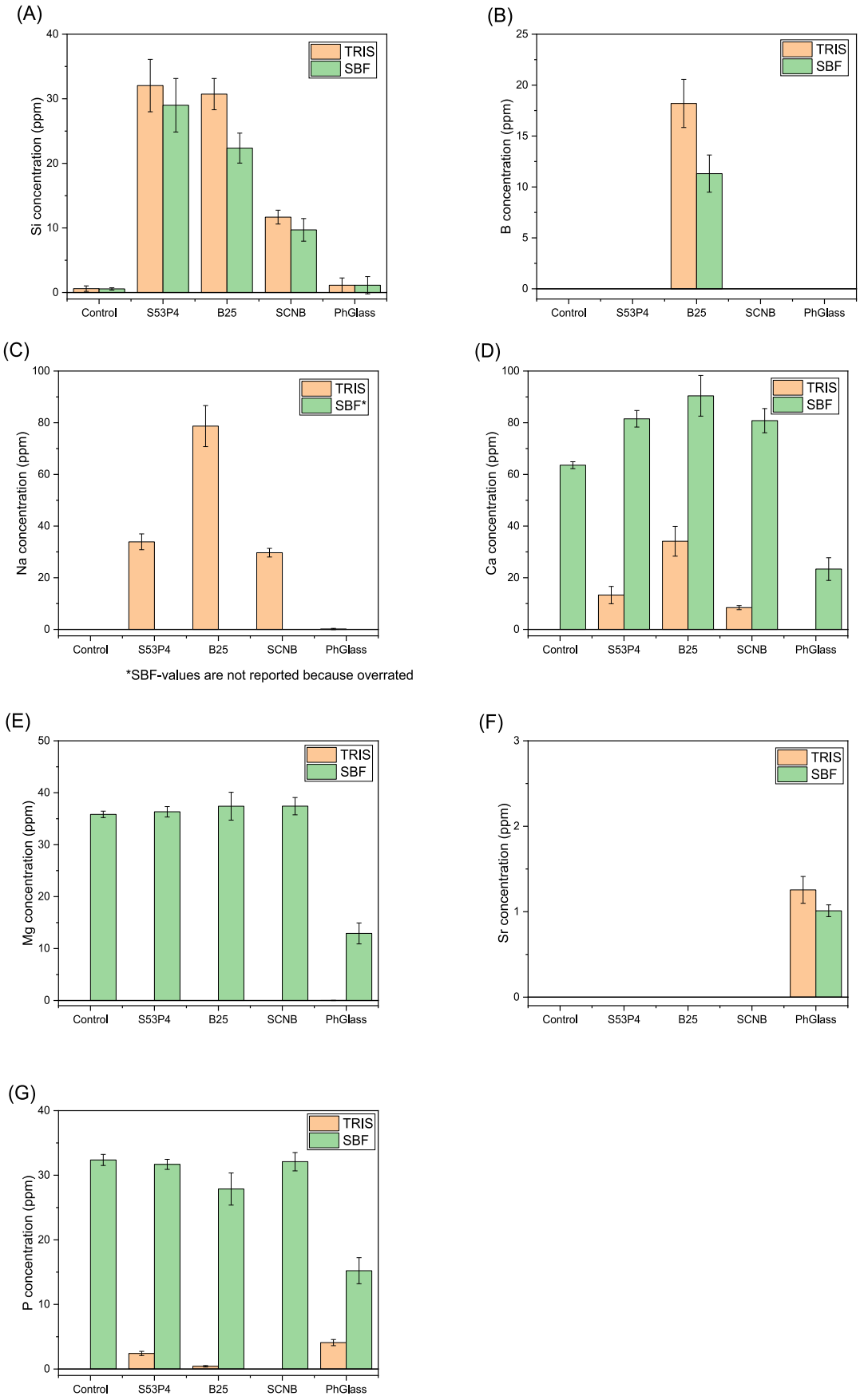

Fig. 7. Post bioactive glass immersion concentration in TRIS and SBF of (A) silicon, (B) boron, (C) sodium, (D) calcium, (E) magnesium, (F) strontium, (G) phosphorus. (For interpretation of the references to colour in this figure legend, the reader is referred to the Web version of this article.)

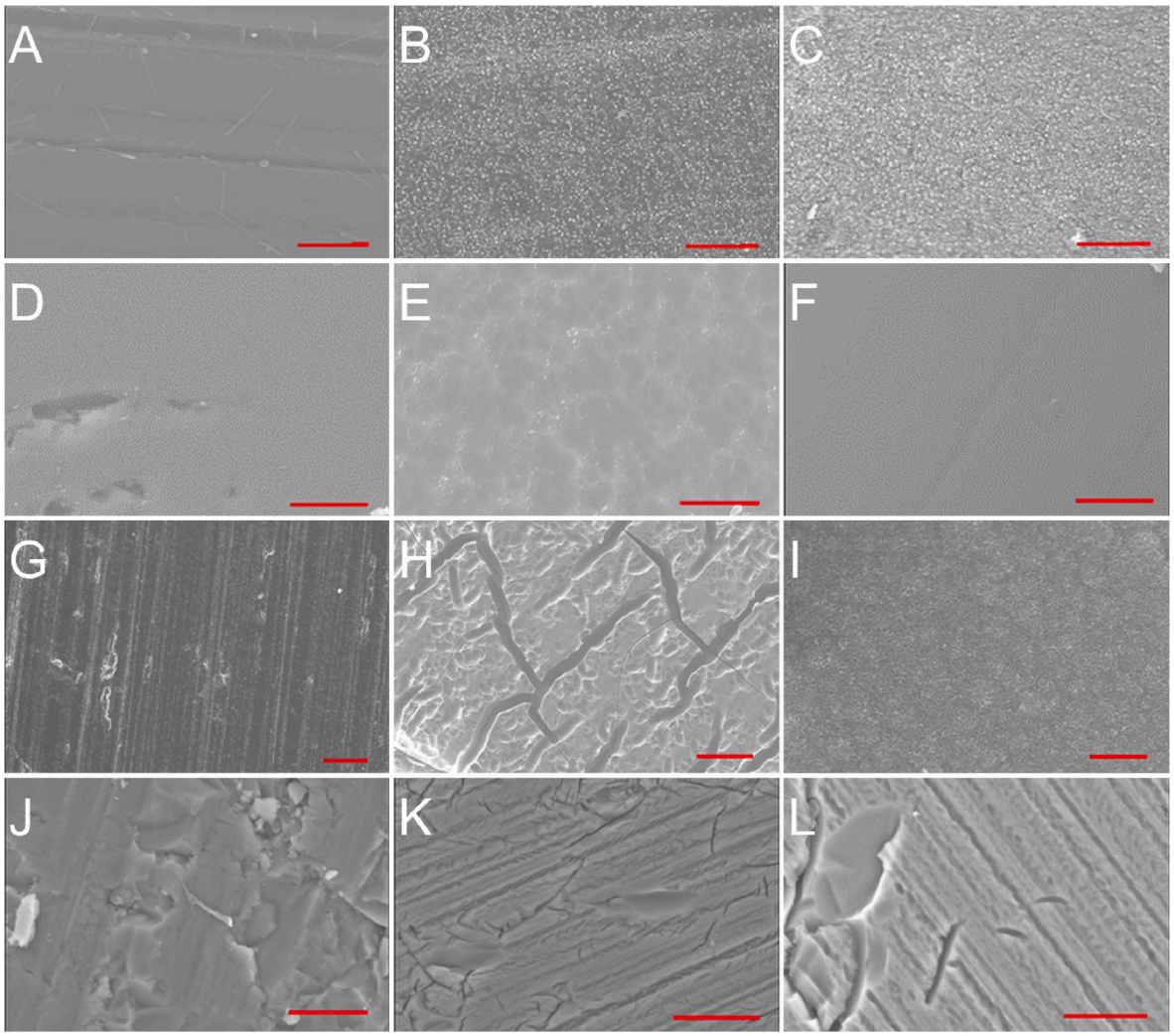

Fig. 8. SEM images on the surface of (A) bare S53P4, (B) TRIS-treated S53P4, (C) SBF-treated S53P4, (D) bare B25, (E) TRIS-treated B25, (F) SBF-treated B25, (G) bare SCNB, (H) TRIS-treated SCNB, (I) SBF-treated SCNB, (J) bare PhGlass, (K) TRIS-treated PhGlass, (L) SBF-treated PhGlass. Scalebar is 4 μm.

crystallized reactive layer precipitated during the soaking process. B25 presents a similar behavior, with grains characterized by a smaller diameter, but more homogeneously distributed. TRIS-treated SCNB shows the formation of a new continuous layer, in which the grains are not distinguishable anymore and a uniform distribution of cracks over this layer is clearly visible.

PhGlass, on the other side, has a different behavior. First of all, the bare samples do not present a surface as smooth as silicate/borosilicate BGs, since it is possible to distinguish some irregularities attributable to a starting phenomenon of surface degradation. Then, after the pre-treatement in both TRIS and SBF, it still possible to visualize the polishing lines, over which some clusters of the precipitated phase are distinguishable. Also in this case, some cracks are present.

The cross sections of the TRIS- and SBF-treated BGs were analyzed by SEM/EDS in order to evaluate 1) the variations of composition at the interface between the glass and the solutions in which they were soaked and 2) the different composition of BGs over their depth. In Fig. 9, the images of the cross sections acquired by SEM are reported, where the path on which EDS analysis was performed is highlighted by a grey line. The EDS analysis is shown in Fig. 10.

TRIS-treated silicate and borosilicate BGs, S53P4 and B25 are characterized by a very thin reactive layer (few μm thick) on the top surface, rich in calcium and phosphorus. Under the reactive layer, a thicker layer rich in silicon is present. TRIS-treated SCNB does not present the reactive layer but only the Si-rich layer. The properties of the Si-rich layer significantly vary between silicate and borosilicate glasses. TRIS-treated S53P4 and SCNB present a thinner layer (around 20 μm thick) with a constant amount of silicon around 90 mol%; TRIS-treated B25 is instead characterized by a thicker Si-rich layer (around 60 μm thick) that is very close to 100 mol%, while the quantity of the other elements is dropping almost to zero. This is in accordance with the previously cited formation of a silica-rich layer on BG surfaces as a result of the 72 h soaking process [22,55,66]. It can be explained by the different reactivity due to the presence of boron in the composition of B25 and to the higher permeability of the matrix to TRIS solution [25]. Furthermore, one must keep in mind that while the glass S53P4 and B25 contain high amount of calcium they also contain phosphorus. It is interesting to note that a short immersion in TRIS (72h) already leads to the saturation of the solution and precipitation of the reactive layer. The concentration in calcium and phosphorus in the reactive layer are consistent with the precipitation of HA/HCA, in agreement with the FTIR analysis. SCNB, in another hand does not contain any phosphorus and thus does not precipitate a reactive layer.

SBF-treated S53P4 and B25 exhibit a significantly thicker reactive layer (10 μm and 20 μm thick, respectively), characterized by a high content of calcium (around 50 mol%) and phosphorus (around 40 mol %). In this case, also SCNB presents a reactive layer, even if thinner (around 5 μm thick), very rich in calcium (around 90 mol%). Ca/P ratio

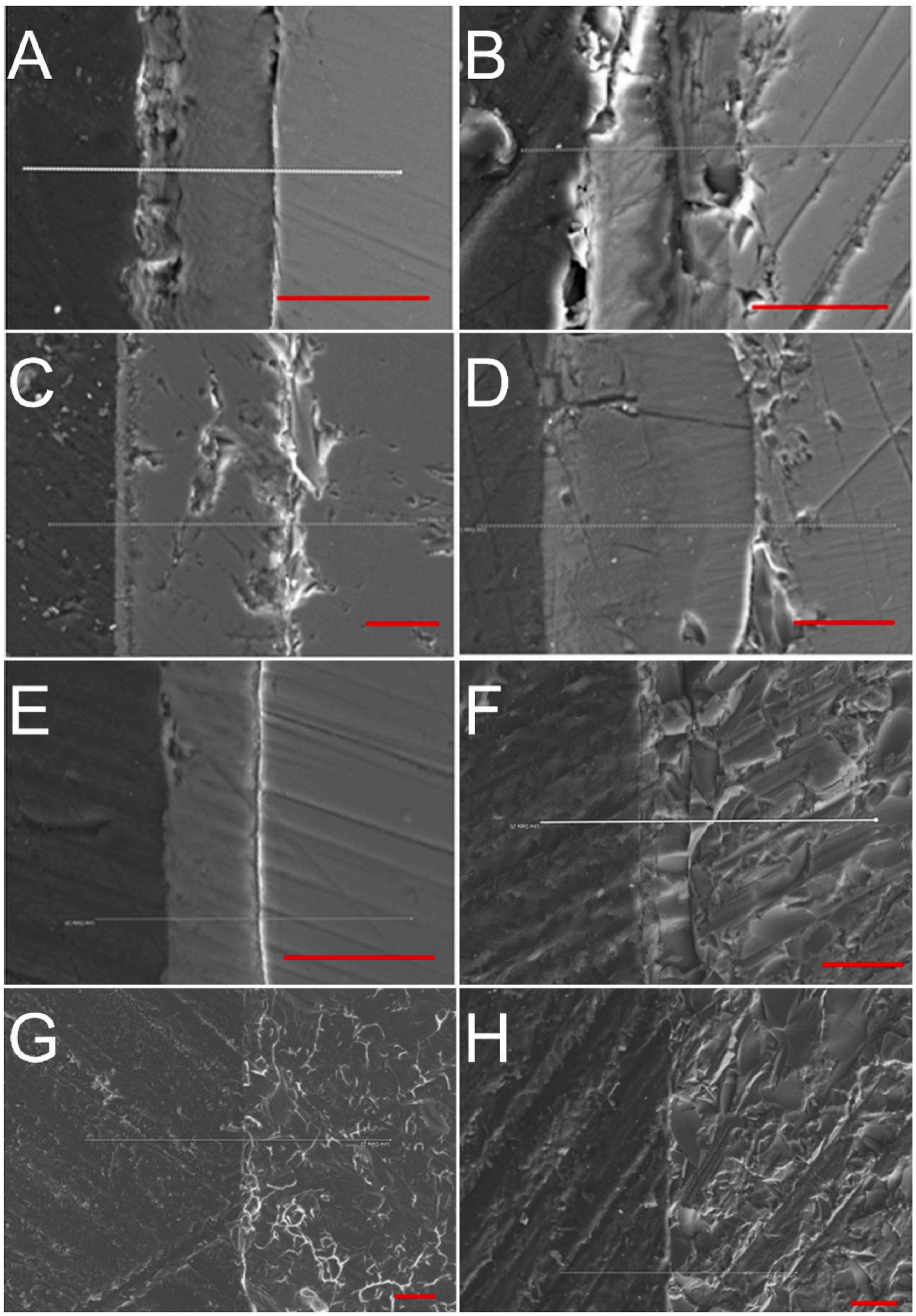

Fig. 9. Cross sections of the TRIS- and SBF-treated BGs acquired by SEM. The grey line constitutes the path through which the EDS analysis was implemented. The images were acquired on (A) TRIS-treated S53P4, (B) SBF-treated S53P4, (C) TRIS-treated B25, (D) SBF-treated B25, (E) TRIS-treated SCNB, (F) SBF-treated SCNB, (G) TRIS-treated PhGlass, (H) SBF-treated PhGlass. Scalebar is 25 μm.

was then calculated over the thickness of the ceramic layer on S53P4 and B25 surfaces, which was (1.64 ± 0.26). This leads to the confirmation of the presence of HA/HCA formation on these BG compositions, as already suggested by FTIR-ATR spectroscopy. Furthermore, the calculated Ca/P ratio has no statistical difference from the theoretical value (1.67) characterizing this material [67]. Under the external HA/HCA layer, the presence of the Si-rich layer is suggested also for SBF-treated samples, with the silicon content ranging from 80 to 100 mol%. On SBF-treated silicate/borosilicate BGs, however, the amount of silicon in the Si-rich layer is slightly lower than in the Si-rich layer of the TRIS-treated ones. In fact, on SBF-treated S53P4 and SCNB, the quantity of Si is around 90 mol%, while on SBF-treated B25 it is around 80 mol%. This can be explained by the different ion release dynamics characterizing BGs when in contact either with TRIS or with SBF solution, leading to the formation of just the Si-rich layer or also to the precipitation of another ceramic phase (HA/HCA) on it [22,55,56,66]. Despite EDS analysis does not show any trace of P at SBF-treated SCNB cross-section, it is still reasonable to believe that HA/HCA precipitated at the surface of this material during the soaking, as confirmed by FTIR-ATR results.

PhGlass reacts differently to the immersion in TRIS and SBF solutions, compared to the silicate/borosilicate BGs. In fact, it is possible to observe a mostly constant composition of PhGlass among its depth, corresponding to the initially set one. The difference of the behavior between silicate/borosilicate BGs and PhGlass is due to the different degradation modality. S53P4, B25 and SCNB are dissolving incongruently, so that the composition is varying at the interface with the environment [8,9]. On the contrary, PhGlass, as a phosphate BG, is dissolving in a congruent way, so that its composition, according to the

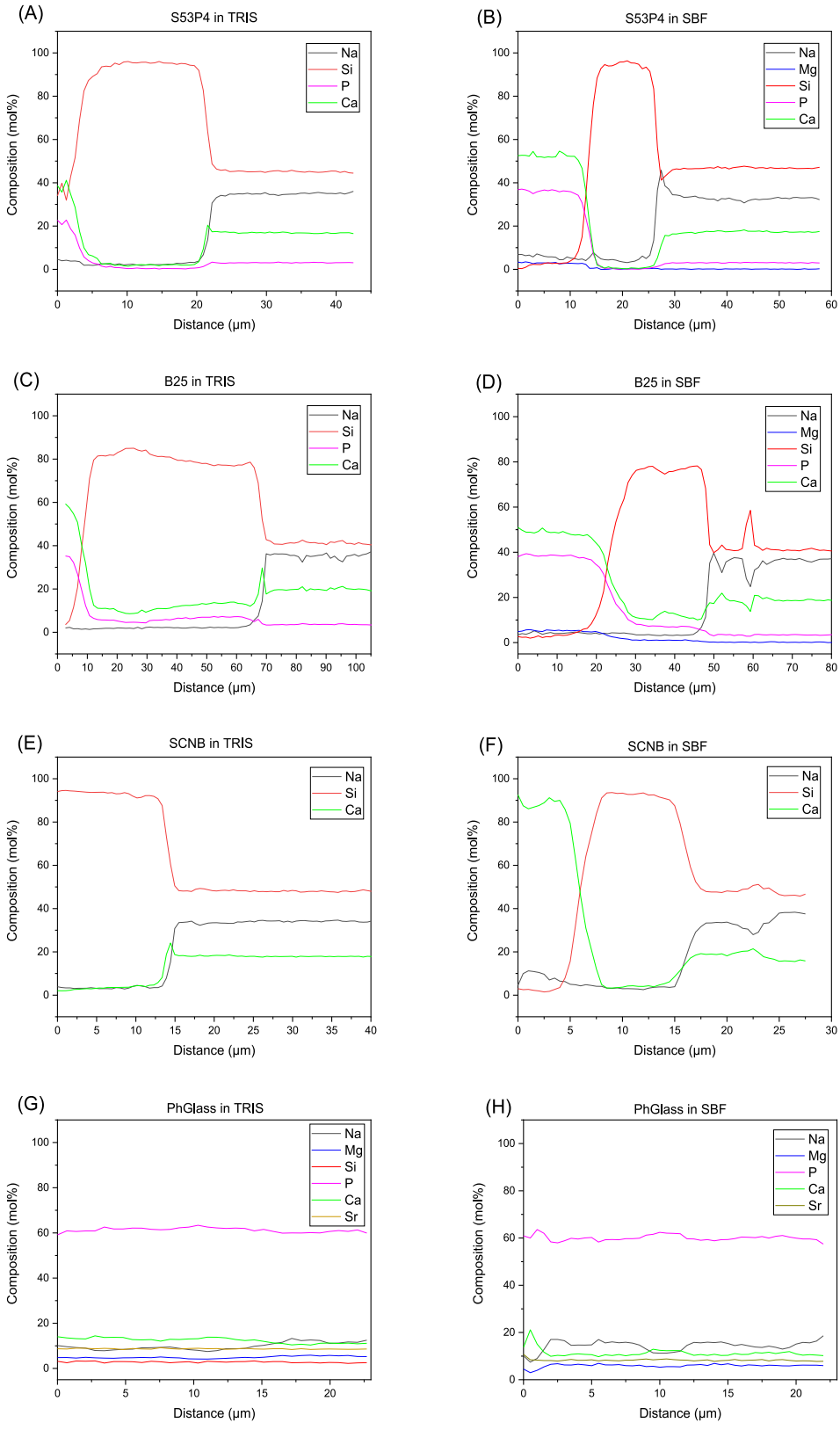

Fig. 10. EDS analysis on the cross sections of (A) TRIS-treated S53P4, (B) SBF-treated S53P4, (C) TRIS-treated B25, (D) SBF-treated B25, (E) TRIS-treated SCNB, (F) SBF-treated SCNB, (G) TRIS-treated PhGlass, (H) SBF-treated PhGlass, going from the surface (distance = 0 μm) to the depth of the bulk material, following the respective paths highlighted in Fig. 6. The results are reported as molar percentage (mol%).

obtained results, remains constant over both its depth and the process [14,15,65].

4. Conclusions

Four BG compositions have been considered in this work, two silicate, one borosilicate and one phosphate glass. They were superficially treated with four different methods: a) 72 h-soaking in TRIS, b) 72 h-soaking in SBF, c) APTES grafting and d) Q-APTES grafting. The aim was to study the impact of the surface modification over their physico-chemical properties. Each surface of interest was characterized and compared with the untreated (bare) one of the respective composition.

Soaking in TRIS and SBF led to a decrease in the surface electronegativity and increased wettability. FTIR and SEM/EDS suggest that a thin and sporadic HA layer forms at the surface of the glass S53P4 and B25 when immersed in TRIS, which is thicker upon soaking in SBF. A reactive layer was also evidenced at the surface of the phosphate glass which can be assigned to dicalcium phosphate dihydrate. The glass SCNB, which does not contain any phosphorus, only presented a HA layer upon soaking in SBF.

Grafting of APTES and Q-APTES was successfully demonstrated by FTIR, where the peaks assigned to aminosilanes were detected. Furthermore, the grafting of the molecules was also evidenced by XPS analysis, showing the presence of nitrogen as well as bromine (for the Q-APTES), at the glasses' surfaces. Silanization led to a decrease in electronegativity, due to the presence of the amine groups, while decreasing the wettability.

Soaking or grafting of molecules enables to have control over the glass surface physico-chemical properties and may be used as a tool to favor/inhibit the adsorption of relevant proteins. In this context, all treated surfaces will be placed in contact with fibronectin and chimeric avidin, used as model proteins, to evidence the impact of such chemical modifications on their adsorption.

Declaration of competing interest

The authors declare the following financial interests/personal relationships which may be considered as potential competing interests: Virginia Alessandra Gobbo reports financial support was provided by Horizon 2020. Virginia Alessandra Gobbo reports a relationship with Horizon 2020 that includes: funding grants.

Acknowledgements

This work was funded by the European Union's Horizon 2020 research and innovation programme under the Marie Skłodowska-Curie grant agreement [No 860462 (PREMUROSA)]. The authors would also like to acknowledge Tampere Microscopy Center for the processing and analysis of the SEM/EDS data.

Appendix A. Supplementary data

Supplementary data to this article can be found online at https://doi.org/10.1016/j.ceramint.2022.09.105.

References

[1] L.L. Hench, Bioglass: 10 milestones from concept to commerce, J. Non-Cryst. Solids 423 (2016) 2–8, https://doi.org/10.1016/j.jnoncrysol.2014.12.038.
[2] V. Miguez-Pacheco, L.L. Hench, A.R. Boccaccini, Bioactive glasses beyond bone and teeth: emerging applications in contact with soft tissues, Acta Biomater. 13 (2015) 1–15, https://doi.org/10.1016/j.actbio.2014.11.004.
[3] M. Schumacher, P. Habibovic, S. van Rijt, Mesoporous bioactive glass composition effects on degradation and bioactivity, Bioact. Mater. 6 (2021) 1921–1931, https://doi.org/10.1016/j.bioactmat.2020.12.007.
[4] L.L. Hench, R.J. Splinter, W.C. Allen, T.K. Greenlee Jr., Bonding mechanisms at the interface of ceramic prosthetic materials, J. Biomed. Mater. Res. 5 (6) (1971) 117–141, https://doi.org/10.1002/jbm.820050611.
[5] N. Gupta, D. Santhiya, S. Murugavel, A. Kumar, A. Aditya, M. Ganguli, S. Gupta, Effects of transition metal ion dopants (Ag, Cu and Fe) on the structural, mechanical and antibacterial properties of bioactive glass, Colloids Surf., A 538 (2018) 393–403, https://doi.org/10.1016/j.colsurfa.2017.11.023.
[6] S. Kargozar, M. Mozafari, S. Ghodrat, E. Fiume, F. Baino, Copper-containing bioactive glasses and glass-ceramics: from tissue regeneration to cancer therapeutic strategies, Mater. Sci. Eng. C 121 (2021), 111741, https://doi.org/10.1016/j.msec.2020.111741.
[7] L.L. Dai, M.L. Mei, C.H. Chu, E.C.M. Lo, Remineralizing effect of a new strontium-doped bioactive glass and fluoride on demineralized enamel and dentine, J. Dent. 108 (2021), 103633, https://doi.org/10.1016/j.jdent.2021.103633.
[8] L. Hupa, S. Fagerlund, J. Massera, L. Björkvik, Dissolution behavior of the bioactive glass S53P4 when sodium is replaced by potassium, and calcium with magnesium or strontium, J. Non-Cryst. Solids 432 (2016) 41, https://doi.org/10.1016/j.jnoncrysol.2015.03.026.
[9] L. Bingel, D. Groh, N. Karpukhina, D.S. Brauer, Influence of dissolution medium pH on ion release and apatiteformation of Bioglass ® 45S5, Mater. Lett. 143 (2015) 279, https://doi.org/10.1016/j.matlet.2014.12.124.
[10] S. Fagerlund, J. Massera, N. Moritz, L. Hupa, M. Hupa, Phase composition and in vitro bioactivity of porous implants made of bioactive glass S53P4, Acta Biomater. 8 (2012) 2331–2339, https://doi.org/10.1016/j.actbio.2012.03.011.
[11] D.C. Clupper, L.L. Hench, Crystallization kinetics of tape cast bioactive glass 45S5, J. Non-Cryst. Solids 318 (2003) 43–48, https://doi.org/10.1016/S0022-3093(02)01857-4.
[12] M. Plewinski, K. Schickle, M. Lindner, A. Kirsten, M. Weber, H. Fischer, The effect of crystallization of bioactive bioglass 45S5 on apatite formation and degradation, Dent. Mater. 29 (2013) 1256, https://doi.org/10.1016/j.dental.2013.09.016.
[13] M.N. Rahaman, D.E. Day, B.S. Bal, Q. Fu, S.B. Jung, L.F. Bonewald, A.P. Tomsia, Bioactive glass in tissue engineering, Acta Biomater. 7 (2011) 2355–2373, https://doi.org/10.1016/j.actbio.2011.03.016.
[14] J. Massera, K. Bourhis, L. Petit, M. Couzi, L. Hupa, M. Hupa, J.J. Videau, T. Cardinal, Effect of the glass composition on the chemical durability of zinc-phosphate-based glasses in aqueous solutions, J. Phys. Chem. Solid. 74 (2013) 121–127, https://doi.org/10.1016/j.jpcs.2012.08.010.
[15] J. Massera, I. Ahmed, L. Petit, V. Aallos, L. Hupa, Phosphate-based glass fiber vs. bulk glass: change in fiber optical response to probe in vitro glass reactivity, Mater. Sci. Eng. C 37 (2014) 251–257, https://doi.org/10.1016/j.msec.2014.01.021.
[16] M. Fabert, N. Ojha, E. Erasmus, M. Hannula, M. Hokka, J. Hyttinen, J. Rocherullé, I. Sigalas, J. Massera, Crystallization and sintering of borosilicate bioactive glasses for application in tissue engineering, J. Mater. Chem. B 5 (23) (2017) 4514–4525, https://doi.org/10.1039/C7TB00106A.
[17] W. Huang, D.E. Day, K. Kittiratanapiboon, M.N. Rahaman, Kinetics and mechanisms of the conversion of silicate (45S5), borate, and borosilicate glasses to hydroxyapatite in dilute phosphate solutions, J. Mater. Sci. Mater. Med. 17 (2006) 583–596, https://doi.org/10.1007/s10856-006-9220-z.
[18] M. Ojansivu, A. Mishra, S. Vanhatupa, M. Juntunen, A. Larionova, J. Massera, S. Miettinen, The effect of S53P4-based borosilicate glasses and glass dissolution products on the osteogenic commitment of human adipose stem cells. https://doi.org/10.1371/journal.pone.0202740, 2018, 13(8).
[19] M. Dzondo, R. Mayap-Nzietchueng, K. Hess, P. Nabet, F. Belleville, B. Dousset, Action of boron at molecular level, Biol. Trace Elem. Res. 85 (2002) 23–33, https://doi.org/10.1385/BTER:85:1:23.
[20] K. Li, X. Lu, I. Razanau, X. Wu, T. Hu, S. Liu, Y. Xie, L. Huang, X. Zheng, The enhanced angiogenic responses to ionic dissolution products from a boron-incorporated calcium silicate coating, Mater. Sci. Eng. C 101 (2019) 513–520, https://doi.org/10.1016/j.msec.2019.04.009.
[21] S. Prasad, S. Datta, T. Adarsh, P. Diwan, K. Annapurna, B. Kundu, K. Biswas, Effect of boron oxide addition on structural, thermal, in vitro bioactivity and antibacterial properties of bioactive glasses in the base S53P4 composition, J. Non-Cryst. Solids 498 (2018) 204–215, https://doi.org/10.1016/j.jnoncrysol.2018.06.027.
[22] I. Notingher, A.R. Boccaccini, J. Jones, V. Maquet, L.L. Hench, Application of Raman microspectroscopy to the characterisation of bioactive materials, Mater. Char. 49 (2003) 255–260, https://doi.org/10.1016/S1044-5803(03)00029-9.
[23] E. Vernè, C. Vitale-Brovarone, E. Bui, C.L. Bianchi, A.R. Boccaccini, Surface functionalization of bioactive glasses, J. Biomed. Mater. Res. 90A (4) (2009) 981–992, https://doi.org/10.1002/jbm.a.32153.
[24] G. Lusvardi, G. Malavasi, L. Menabue, S. Shruti, Gallium-containing phosphosilicate glasses: functionalization and in-vitro bioactivity, Mater. Sci. Eng. C 33 (6) (2013) 3190–3196, https://doi.org/10.1016/j.msec.2013.03.046.
[25] S. Ferraris, A. Nommeots-Nomm, S. Spriano, E. Vernè, J. Massera, Surface reactivity and silanization ability of borosilicate and Mg-Sr-based bioactive glasses, Appl. Surf. Sci. 475 (2019) 43–55, https://doi.org/10.1016/j.apsusc.2018.12.218.
[26] S. Chitra, P. Bargavi, M. Balasubramaniam, R.R. Chandran, S. Balakumar, Impact of copper on in-vitro biomineralization, drug release efficacy and antimicrobial properties of bioactive glasses, Mater. Sci. Eng. C 109 (2020), 110598, https://doi.org/10.1016/j.msec.2019.110598.
[27] B. Thavornyutikarn, B. Feltis, P.F.A. Wright, T.W. Turney, Effect of pre-treatment of crystallized bioactive glass with cell culture media on structure, degradability, and biocompatibility, Mater. Sci. Eng. C 97 (2019) 188–197, https://doi.org/10.1016/j.msec.2018.12.034.
[28] M. Miola, C. Vitale-Brovarone, C. Mattu, E. Vernè, Antibiotic loading on bioactive glasses and glass-ceramics: an approach to surface modification, J. Biomater. Appl. 28 (2) (2012) 308–319, https://doi.org/10.1177/0885328212447665.
[29] F.E. Ciraldo, E. Boccardi, V. Melli, F. Westhauser, A.R. Boccaccini, Tackling bioactive glass excessive in vitro bioreactivity: preconditioning approaches for cell

culture tests, Acta Biomater. 75 (2018) 3–10, https://doi.org/10.1016/j.actbio.2018.05.019.
[30] A.C. Marsh, N.P. Mellott, M. Crimp, A. Wren, N. Hammer, X. Chatzistavrou, Ag-doped bioactive glass-ceramic 3D scaffolds: microstructural, antibacterial, and biological properties, J. Eur. Ceram. Soc. 41 (6) (2021) 3717–3730, https://doi.org/10.1016/j.jeurceramsoc.2021.01.011.
[31] T. Tite, A.C. Popa, B.W. Stuart, H.R. Fernandes, I.M. Chirica, G.A. Lungu, D. Macovei, C. Bartha, L. Albulescu, C. Tanase, S. Nita, N. Rusu, D.M. Grant, J.M. F. Ferreira, G.E. Stan, Independent and complementary bio-functional effects of CuO and Ga_2O_3 incorporated as therapeutic agents in silica- and phosphate-based bioactive glasses, J.Materiomics (2022), https://doi.org/10.1016/j.jmat.2021.12.009.
[32] C. Gruian, E. Vanea, S. Simon, V. Simon, FTIR and XPS studies of protein adsorption onto functionalized bioactive glass, Biochim. Biophys. Acta, Proteins Proteomics 1824 (7) (2012) 873–881, https://doi.org/10.1016/j.bbapap.2012.04.008.
[33] N.B. Hyunh, C. Santos Dias Palma, R. Rahikainen, A. Mishra, L. Azizi, E. Vernè, S. Ferraris, V.P. Hytönen, A. Sanches Ribeiro, J. Massera, Surface modification of bioresorbable phosphate glasses for controlled protein adsorption, ACS Biomater. Sci. Eng. 7 (9) (2021) 4483–4493, https://doi.org/10.1021/acsbiomaterials.1c00735.
[34] T. Kokubo, K. Hata, T. Nakamura, T. Yamamuro, Apatite formation on ceramics, metals and polymers induced by CaO SiO_2 based glass in a simulated body fluid, in: Bioceramics, Proceedings of the 4th International Symposium on Ceramics in Medicine London, UK, September, 1991, pp. 113–120, https://doi.org/10.1016/B978-0-7506-0269-3.50020-7.
[35] J. Massera, A. Mishra, S. Guastella, S. Ferraris, E. Vernè, Surface functionalization of phosphate-based bioactive glasses with 3-aminopropyltriethoxysilane (APTS), Biomedical Glasses 2 (2016) 51–62, https://doi.org/10.1515/bglass-2016-0007.
[36] A. Deraine, M.T. Rebelo Calejo, R. Agniel, M. Kellomäki, E. Pauthe, M. Boissière, J. Massera, Polymer-based honeycomb films on bioactive glass: toward a biphasic material for bone tissue engineering applications, ACS Appl. Mater. Interfaces 13 (25) (2021) 29984–29995, https://doi.org/10.1021/acsami.1c03759.
[37] S.A. Cerneaux, S.M. Zakeeruddin, M. Grätzel, Y.B. Cheng, L. Spiccia, New functional triethoxysilanes as iodide sources for dye-sensitized solar cells, J. Photochem. Photobiol. Chem. 198 (2–3) (2008) 186–191, https://doi.org/10.1016/j.jphotochem.2008.03.008.
[38] N. Fairley, V. Fernandez, M. Richard-Plouet, C. Guillot-Deudon, J. Walton, E. Smith, D. Flahaut, M. Greiner, M. Biesinger, S. Tougaard, D. Morgan, J. Baltrusaitis, Systematic and collaborative approach to problem solving using X-ray photoelectron spectroscopy, Appl. Surf. Sci. Adv. 5 (2021), 100112, https://doi.org/10.1016/j.apsadv.2021.100112.
[39] G. Riccucci, M. Cazzola, S. Ferraris, V.A. Gobbo, M. Miola, A. Bosso, G. Örlygsson, C.H. Ng, E. Vernè, S. Spriano, Surface functionalization of bioactive glasses and hydroxyapatite with polyphenols from organic red grape pomace, J. Am. Ceram. Soc. 105 (3) (2021) 1697–1710, https://doi.org/10.1111/jace.17849.
[40] S. Ferraris, S. Yamaguchi, N. Barbani, C. Cristallini, G. Gautier di Confiego, J. Barberi, M. Cazzola, M. Miola, E. Vernè, S. Spriano, The mechanical and chemical stability of the interfaces in bioactive materials: the substrate-bioactive surface layer and hydroxyapatite-bioactive surface layer interfaces, Mater. Sci. Eng. C 116 (2020), 111238, https://doi.org/10.1016/j.msec.2020.111238.
[41] J. Xu, C. Wang, S. Zhou, R. Zhang, Y. Tian, Low temperature direct bonding of Si and quartz glass using the APTES modification, Ceram. Int. 45 (13) (2019) 16670–16675, https://doi.org/10.1016/j.ceramint.2019.05.098.
[42] Y. Sun, M. Yanagisawa, M. Kunimoto, M. Nakamura, T. Homma, Depth profiling of APTES self-assembled monolayers using surface-enhanced confocal Raman microspectroscopy, Spectrochim. Acta Mol. Biomol. Spectrosc. 184 (2017) 1–6, https://doi.org/10.1016/j.saa.2017.04.036.
[43] R.G. Acres, A.V. Ellis, J. Alvino, C.E. Lenahan, D.A. Khodakov, G.F. Metha, G.G. Andersson, Molecular structure of 3-aminopropyltriethoxysilane layers formed on silanol-terminated silicon surfaces, J. Phys. Chem. C, 116:6289-6297. https://doi.org/10.1021/jp212056s.
[44] NIST X-Ray Photoelectron Spectroscopy Database, Version 4.1, National Institute of Standards and Technology, Gaithersburg, 2012. http://srdata.nist.gov/xps/.
[45] A. Mohtasebi, T. Chowdhuri, L.H.H. Hsu, M.C. Biesinger, P. Kruse, Interfacial charge transfer between phenyl-capped aniline tetramer films and iron oxide surfaces, J. Phys. Chem. C 120 (51) (2016) 29248–29263, https://doi.org/10.1021/acs.jpcc.6b09950.
[46] A. Majjane, A. Chahine, M. Et-tabirou, B. Echchahed, T.-O. Do, P. Mc Breen, X-ray photoelectron spectroscopy (XPS) and FTIR studies of vanadium barium phosphate glasses, Mater. Chem. Phys. 143 (2) (2014) 779–787, https://doi.org/10.1016/j.matchemphys.2013.10.013.
[47] C. Haensch, S. Hoeppener, U.S. Schubert, Chemical surface reactions by click chemistry: coumarin dye modification of 11-bromoundecyltrichlorosilane monolayers, Nanotechnology 19 (3) (2008), 035703, https://doi.org/10.1088/0957-4484/19/03/035703.
[48] J. Massera, L. Hupa, Influence of SrO substitution for CaO on the properties of bioactive glass S53P4, J. Mater. Sci. Mater. Med. 25 (2014) 657–668, https://doi.org/10.1007/s10856-013-5120-1.
[49] N. Nematidil, M. Sadeghi, S. Nezami, H. Sadeghi, Synthesis and characterization of Schiff-base based chitosan-g-glutaraldehyde/NaMMTNPs-APTES for removal Pb^{2+} and Hg^{2+} ions, Carbohydr. Polym. 222 (2021), 114971, https://doi.org/10.1016/j.carbpol.2019.114971.
[50] X. Guo, H. Yuan, T. Xiao, Y. Wu, Application of micro-FTIR spectroscopy to study molecular association of adsorbed water with lignin, Int. J. Biol. Macromol. 131 (2019) 1038–1043, https://doi.org/10.1016/j.ijbiomac.2019.03.193.
[51] J.K. Odusote, Y. Danyuo, A.D. Baruwa, A.A. Azeez, Synthesis and characterization of hydroxyapatite from bovine bone for production of dental implants, J. Appl. Biomater. Funct. Mater. 17 (2) (2019), https://doi.org/10.1177/2280800019836829, 2280800019836829.
[52] N. Sebeia, M. Jabli, A. Ghith, [λ-Carrageenan-calcium phosphate] and [sodium alginate-calcium phosphate] modified with dimethyl diallyl ammonium chloride and diallylamin co-polymer as efficient adsorbents of anionic dyes, Int. J. Biol. Macromol. 126 (2019) 641–652, https://doi.org/10.1016/j.ijbiomac.2018.12.260.
[53] Ö.H. Andersson, I. Kangasniemi, Calcium phosphate formation at the surface of bioactive glass in vitro, J. Biomed. Mater. Res. 25 (8) (1991) 1019–1030, https://doi.org/10.1002/jbm.820250808.
[54] S.V. Sirkiä, M. Nakamura, S. Qudsia, M. Siekkinen, J.-H. Smått, J. Peltonen, T. J. Heino, L. Hupa, P.K. Vallittu, Structural and elemental characterization of glass and ceramic particles for bone surgery, Dent. Mater. 37 (9) (2021) 1350–1357, https://doi.org/10.1016/j.dental.2021.06.004.
[55] S. Ferraris, S. Yamaguchi, N. Barbani, M. Cazzola, C. Cristallini, M. Miola, E. Vernè, S. Spriano, Bioactive materials: in vitro investigation of different mechanisms of hydroxyapatite precipitation, Acta Biomater. 102 (2020) 468–480, https://doi.org/10.1016/j.actbio.2019.11.024.
[56] J.R. Jones, O. Tsigkou, E.E. Coates, M.M. Stevens, J.M. Polak, L.L. Hench, Extracellular matrix formation and mineralization on a phosphate-free porous bioactive glass scaffold using primary human osteoblast (HOB) cells, Biomaterials 28 (9) (2007) 1653–1663, https://doi.org/10.1016/j.biomaterials.2006.11.022.
[57] P. Saengdee, C. Promptmas, S. Thanapitak, A. Srisuwan, A. Pankiew, N. Thornyanadacha, W. Chaisrirantanakul, E. Chaowicharat, W. Jeamsaksiri, Optimization of 3-aminopropyltriethoxysilane functionalization on silicon nitride surface for biomolecule immobilization, Talanta 207 (2020), 120305, https://doi.org/10.1016/j.talanta.2019.120305.
[58] H. Ungan, A. Bayrakçeken Yurtcan, Water management improvement in PEM fuel cells via addition of PDMS or APTES polymers to the catalyst layer, Turk. J. Chem. 44 (5) (2020) 1227–1243, https://doi.org/10.3906/kim-2002-49.
[59] A. Saitoh, R.K. Brow, U. Hoppe, G. Tricot, S. Anan, H. Takebe, The structure and properties of xZnO–(67-x)SnO–P2O5 glasses: (I) optical and thermal properties, Raman and infrared spectroscopies, J. Non-Cryst. Solids 484 (2018) 132–138, https://doi.org/10.1016/j.jnoncrysol.2018.01.030.
[60] A. Sroka-Bartnicka, L. Borkowski, G. Ginalska, A. Ślósarczyk, S.G. Kazarian, Structural transformation of synthetic hydroxyapatite under simulated in vivo conditions studied with ATR-FTIR spectroscopic imaging, Spectrochim. Acta Mol. Biomol. Spectrosc. 171 (2017) 155–161, https://doi.org/10.1016/j.saa.2016.07.051.
[61] N. Jmal, J. Bouaziz, Synthesis, characterization and bioactivity of a calcium-phosphate glass-ceramics obtained by the sol-gel processing method, Mater. Sci. Eng. C 71 (2017) 279–288, https://doi.org/10.1016/j.msec.2016.09.058.
[62] S. Prasad, A. Gaddam, A. Jana, S. Kant, P.K. Sinha, S. Tripathy, K. Annapurna, J.M. F. Ferreira, A.R. Allu, K. Biswas, Structure and stability of high CaO- and P_2O_5-containing silicate and borosilicate bioactive glasses, J. Phys. Chem. 123 (35) (2019) 7558–7569, https://doi.org/10.1021/acs.jpcb.9b02455.
[63] H. Miyoshi, D. Chen, H. Masui, T. Yazawa, T. Akai, Effect of calcium additive on structural changes under heat treatment in sodium borosilicate glasses, J. Non-Cryst. Solids 345–346 (2004) 99–103, https://doi.org/10.1016/j.jnoncrysol.2004.08.003.
[64] J.M. Tainio, D.A. Avila Salazar, A. Nommeots-Nomm, C. Roiland, B. Bureau, D. R. Neuville, D.S. Brauer, J. Massera, Structure and in vitro dissolution of Mg and Sr containing borosilicate bioactive glasses for bone tissue engineering, J. Non-Cryst. Solids 533 (2020), 119893, https://doi.org/10.1016/j.jnoncrysol.2020.119893.
[65] B.C. Bunker, G.W. Arnold, J.A. Wilder, Phosphate glass dissolution in aqueous solutions, J. Non-Cryst. Solids 64 (3) (1984) 291–316, https://doi.org/10.1016/0022-3093(84)90184-4.
[66] T. Kokubo, Design of bioactive bone substitutes based on biomineralization process, Mater. Sci. Eng. C 25 (2005) 97–104, https://doi.org/10.1016/j.msec.2005.01.002.
[67] H. Wang, J.K. Lee, A. Moursi, J.J. Lannutti, Ca/P ratio effects on the degradation of hydroxyapatite *in vitro*, J. Biomed. Mater. Res. 67A (2) (2003) 599–608, https://doi.org/10.1002/jbm.a.10538.